AIP Journal of Applied Physics

High surface area electrodes in ionic polymer transducers: Numerical and experimental investigations of the electro-chemical behavior

Barbar J. Akle, Wassim Habchi, Thomas Wallmersperger, Etienne J. Akle, and Donald J. Leo

Citation: Journal of Applied Physics **109**, 074509 (2011); doi: 10.1063/1.3556751
View online: http://dx.doi.org/10.1063/1.3556751
View Table of Contents: http://scitation.aip.org/content/aip/journal/jap/109/7?ver=pdfcov
Published by the AIP Publishing

High surface area electrodes in ionic polymer transducers: Numerical and experimental investigations of the electro-chemical behavior

Barbar J. Akle,[1,a)] Wassim Habchi,[1] Thomas Wallmersperger,[2] Etienne J. Akle,[3] and Donald J. Leo[3]
[1]*Department of Industrial and Mechanical Engineering, Lebanese American University, Byblos, Lebanon*
[2]*Institut für Festkörpermechanik, Technische Universität Dresden, Dresden 01062, Germany*
[3]*Center for Intelligent Materials Systems and Structures, Virginia Polytechnic Institute and State University, Blacksburg, Virginia 24061, USA*

(Received 18 May 2010; accepted 23 January 2011; published online 7 April 2011)

Ionomeric polymer transducer (IPT) is an electroactive polymer that has received considerable attention due to its ability to generate large bending strain (>5%) and moderate stress at low applied voltages (±2 V). Ionic polymer transducers consist of an ionomer, usually Nafion, sandwiched between two electrically conductive electrodes. A novel fabrication technique denoted as the direct assembly process (DAP) enabled controlled electrode architecture in ionic polymer transducers. A DAP built transducer consists of two high surface area electrodes made of electrically conducting particles uniformly distributed in an ionomer matrix sandwiching an ionomer membrane. The purpose of this paper is to investigate and simulate the effect of these high surface area particles on the electro-chemical response of an IPT. Theoretical investigations as well as experimental verifications are performed. The model used consists of a convection-diffusion equation describing the chemical field as well as a Poisson equation describing the electrical field. The two-dimensional model incorporates highly conductive particles randomly distributed in the electrode area. Traditionally, these kinds of electrodes were simulated with boundary conditions representing flat electrodes with a large dielectric permittivity at the polymer boundary. This model enables the design of electrodes with complicated geometrical patterns. In the experimental section, several transducers are fabricated using the DAP process on Nafion 117 membranes. The architecture of the high surface area electrodes in these samples is varied. The concentration of the high surface area RuO_2 particles is varied from 30 vol% up to 60 vol% at a fixed thickness of 30 μm, while the overall thickness of the electrode is varied from 10 μm up to 40 μm at a fixed concentration of 45%. The flux and charge accumulation in the materials are measured experimentally and compared to the results of the numerical simulations. Trends of the experimental and numerical investigations are in agreement, while the computational capacity is limiting the ability to add sufficient amount of metal particle to the electrode in order to match the magnitudes. © *2011 American Institute of Physics*. [doi:10.1063/1.3556751]

I. INTRODUCTION

Ionomeric polymer transducers, also called ionic polymer-metal composites (IPMC), are transducers that exhibit electro-mechanical actuation and sensing properties. It is well established that ionomer materials, when properly plated with conductive metal on their surfaces, exhibit a bending deformation due to an applied voltage across the thickness.[1,2] Equally, the materials exhibit an electric sensing response when the material is mechanically deformed.[3,4] These properties allow them to be used as electro-mechanical sensors and actuators. In comparison to other types of materials that exhibit electro-mechanical coupling, such as piezoelectric materials, ionomeric materials have been shown to produce bending strains on the order of 5% under the application of potentials of less than 4 V (Ref. 5). Recent advances in the development of 'dry' materials have also enabled the use of these ionomeric materials in air,[6,7] thus increasing the practicality of using these materials in environments that do not require control over hydration or humidity. Furthermore, ionic polymer transducers are tested to be reliable for over 10^6 cycles.[8]

Shown in Fig. 1 is an ionomeric polymer transducer (IPT) that consists of a solid electrolyte, usually Nafion or Flemion, sandwiched between two conductive electrodes. The conductive electrodes are made of a mixture of high surface area conductive particles diffused in a matrix of the polymer electrolyte. Recently, it has been shown in both experiment and theory that the electrode layer is a critical component that strongly influences transducer performance. Experimental work has correlated the actuation properties of the transducer to its measured capacitance.[9] This result was consistent for ionomers with substantial differences in composition; therefore it strongly suggests that charge accumulation at the polymer-metal interface is a determining factor in the strain and strain rate generated during actuation.

Although a number of advances have been made in the development of ionomeric transducers in recent years, there

a)Electronic mail: barbar.akle@lau.edu.lb.

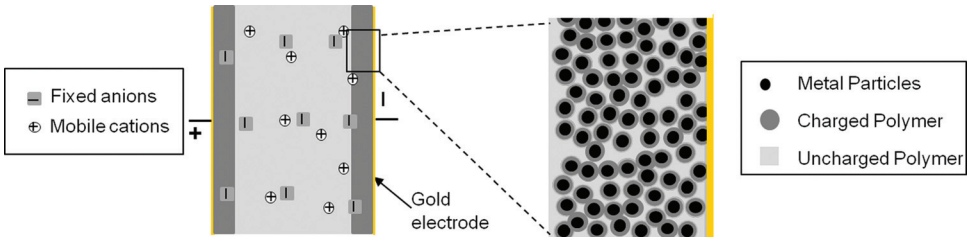

FIG. 1. (Color online) Schematic of an IPT strip showing the fixed anions uniformly distributed while the mobile cations aggregating toward the cathode (left) and a schematic of a typical electrode in an IPT showing the charge accumulation around the conductive particles (right).

still remains a gap in understanding the fundamental mechanisms that promote electro-mechanical coupling. It has been well established for a number of years that the electro-mechanical coupling in these transducers is due to the ion conduction in the polymer. Beyond that, though, there have been a number of models based on different physical phenomena that can closely match experimental data.

The models that provide a direct comparison between experiment and theory can generally be separated into phenomenological models based on curvefits of experimental data,[10–14] and physics-based models that attempt to predict the material response from governing equations.[15–22]

In the present paper, both theoretical and experimental investigations of ionic polymer transducers with high surface area electrodes are performed. The numerical model can capture the electro-chemical behavior in the polymer membrane and in the electrode region. As compared to previous work, this study expands the electro-mechanical models to the two-dimensional case and enables the incorporation of the conductive particles in the electrodes. Traditionally, these kinds of electrodes were simulated with boundary conditions representing flat electrodes with a large dielectric permittivity at the polymer boundary.[23–25] Aureli *et al.*[23] and Porfiri[26] presented a closed-form model that uses perturbation methods to simulate the electrode roughness. The model presented in this study additionally enables the design of the distribution of particles throughout the high surface area electrodes.

This paper is organized as follows: In Sec. II the electro-chemical model developed by Wallmersperger *et al.*[16,27] is presented in a short form along with the additions needed for two-dimensional case. In Sec. III, the model and the mesh of the IPT are calibrated and compared to published data. The results from the numerical simulations of several IPTs with varied electrode architectures are discussed in Sec. IV. The experimental procedures are presented in Sec. V, while the measurements from the several transducers that are fabricated using the direct assembly process on Nafion 117 membranes are shown in Sec. VI. Finally, Sec. VII concludes and summarizes the findings of this work.

II. MODELING

The multi-field model introduced in this section describes the electro-chemical behavior inside an ionic polymer transducer.[27] The formulation allows the computation of the space-time distribution of the electric potential and ionic concentration in the material.

A. Chemical field

The formulation for the chemical field is based on the balance equation for the flux of the mobile ions and fixed charges. Using the conservation of mass and the Nernst-Planck equation for the flux, the convection-diffusion equation for each species

$$\dot{c}_\alpha = \left[D_\alpha c_{\alpha,i} + z_\alpha c_\alpha \mu_\alpha \Psi_{,i}\right]_{,i} \tag{1}$$

is obtained. The variable c_α is the concentration of the species α while D_α is the diffusion constant, $\mu_\alpha = (F/RT)D_\alpha$ is the unsigned mobility, z_α is the valence of the ions, and Ψ is the electric potential. $\partial/\partial x_i$ is the gradient in space and denotes the partial derivative with respect to x_i. $\dot{c}_\alpha$ is the first derivative in time of the concentration c_α.

B. Electrical field

The electric field is described by the quasi-static Poisson equation

$$\Psi_{,ii} = -\frac{F}{\varepsilon\varepsilon_0}\sum_{\alpha=1}^{N_f+N_b}(z_\alpha c_\alpha), \tag{2}$$

where ε_0 is the permittivity of free space, ε is the relative dielectric constant, and F is the Faraday constant ($F = N_A \cdot e = 96\,487$ C/mol), where N_A is the Avogadro constant and e is the electric elementary charge. N_f and N_b denote the number of freely movable species and the number of bound species, respectively.

C. Boundary conditions at the electrodes

In order to solve the given equations, boundary conditions for both the chemical and electrical field have to be specified. For the electric field, the electric potential is prescribed at both domain boundaries (electrode and particles). For the chemical field, a zero-flux boundary condition [$J_i(x_i, y_i, t) = 0$] is imposed over the polymer-electrode interface. This results in the following equation:

$$-D_\alpha c_{\alpha,i} - \frac{F}{RT} z_\alpha D_\alpha c_\alpha \Psi_{,i} = 0. \tag{3}$$

A symmetry boundary condition is applied on the remaining boundaries ($y = 0$ and $y = h$).

D. Non-dimensional analysis

The previously defined equations are all solved in their dimensionless form. This allows the use of a unique geometrical domain to represent different IPT thicknesses. In addition, the different unknowns of the problem are scaled to the same order of magnitude providing a better conditioned

system of equations. The different variables of the problem are scaled to unity by defining the dimensionless parameters

$$\bar{x} = \frac{x}{h}, \bar{y} = \frac{y}{h}, \bar{w} = \frac{w}{h}, \bar{\Psi} = \frac{\Psi}{\Psi_0}, \text{ and } \bar{c}_\alpha = \frac{c_\alpha}{c^-},$$

where h is defined as the thickness of an IPT actuator, and w the width (see Fig. 2). Note that the electric potential Ψ does not require any scaling and it was scaled by $\Psi_0 = 1\text{V}$ for the sake of consistency. The resulting dimensionless equations are

$$h^2 \dot{\bar{c}}_\alpha = \left[D_\alpha \bar{c}_{\alpha,\bar{i}} + z_\alpha \bar{c}_\alpha \mu_\alpha \bar{\Psi}_{,\bar{i}} \right]_{,\bar{i}}, \tag{4}$$

$$\bar{\Psi}_{,\bar{i}\bar{i}} = -h^2 c^- \frac{F}{\varepsilon\varepsilon_0} \sum_{\alpha=1}^{N_f+N_b} (z_\alpha \bar{c}_\alpha), \tag{5}$$

and finally, the dimensionless boundary condition for the chemical problem is

$$- D_\alpha \bar{c}_{\alpha,\bar{i}} - \frac{F}{RT} z_\alpha D_\alpha \bar{c}_\alpha \bar{\Psi}_{,\bar{i}} = 0, \tag{6}$$

while the fixed boundary conditions of the electrical problem remain unchanged since the electric field is scaled to 1 V.

E. Current density and charge density

The ion transport in the polymer is directly related to the charge density (distribution)

$$\rho(\bar{x}_{\bar{i}}, \bar{y}_{\bar{i}}, t) = F c^- \sum_{\alpha=1}^{N_f+N_b} [z_\alpha \bar{c}_\alpha(\bar{x}_{\bar{i}}, \bar{y}_{\bar{i}}, t)]. \tag{7}$$

The surface charge per unit area, $q^s(t)$, induced by the existence of a nonzero charge density ρ within the sample is obtained by an integration in the x-(thickness) direction

$$q^s(t) = \int_\Omega \rho x \, d\Omega \,. \tag{8}$$

The integration is applied according to Ref. 28.

The resulting current per unit area is the time derivative of the induced surface charge,

$$i(t) = \frac{dq^s(t)}{dt}. \tag{9}$$

The surface charge and current are computed by Eqs. (8) and (9), respectively.

III. NUMERICAL MODEL

In this section, the numerical model and its calibration are presented for the one dimensional model, one-dimensional model with decreased dielectric constant, the two-dimensional model, and finally the two-dimensional model including particles.

A. Model description

The dimensionless chemical and electrical Eqs. (1) and (2) are solved using the finite element method. The geometrical domain Ω is defined as a straight line for the one-dimensional case and a rectangle of width w and length h for the two-dimensional case (see Fig. 2). The two equations are solved simultaneously in a fully-coupled scheme. This avoids any loss of information that might occur with a weak coupling procedure and a consequent degradation in the convergence rate. However, the system of equations becomes nonlinear, requiring a Newton-like procedure for its resolution. The linearized system of equations is solved at every Newton iteration using the UMFPACK direct solver.[29] The time stepping scheme is based on the BDF (Backward Differential Formula) method.[30] Finally, variable nonstructured triangular meshing of the geometrical domain is used. The latter is refined around the electrodes and the particles, providing a higher precision in these areas where the solution exhibits sharper gradients as shown in Fig. 2. Note that a certain clearance area near the top and bottom boundaries is left particle-free in order to avoid any boundary effects on the solution. For further details regarding the technical aspects of the finite element method (FEM) the reader is referred to any of the classical FEM handbooks.[31,32]

B. Model calibration

The calibration procedure is realized in three steps. First, the one-dimensional model is calibrated against the results published in Wallmersperger *et al.*;[28] then the two-dimensional model is compared to the one-dimensional model for the same set of parameters which are listed in Table I. Finally, the model is calibrated for the two-dimensional case including particles.

For the one-dimensional case, Figs. 3(a) and 3(b) show the normalized spatial charge density on the cathode and the anode respectively for an applied potential of 50, 200, and 500 mV. These results are in total agreement with the numerical simulations reported in Wallmersperger *et al.*[28] Furthermore, the asymmetric shape of these numerical simulations is in close agreement with the analytical results reported in

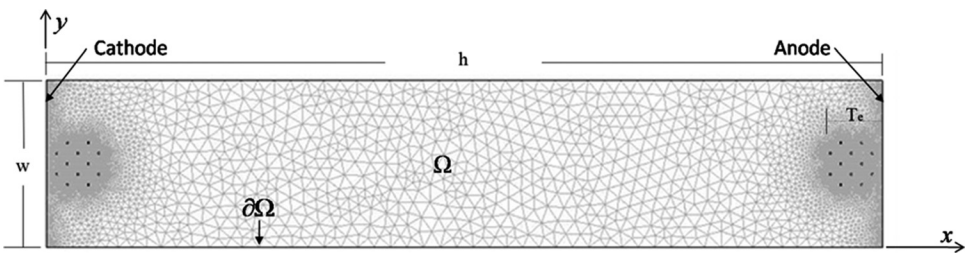

FIG. 2. The mesh of an IPT actuator with 12 particles on each side of the electrodes.

TABLE I. Simulation parameters.

Parameter	Variable	Value
Polymer thickness	h	200 μm
Anion Concentration	c^-	1073 mol/m^3
Diffusion Coefficient	D_α	$6 \cdot 10^{-11}$ m^2/s
Dielectric Constant	$\varepsilon\varepsilon_0$	17.7 (or 1.77) mF/m
Temperature	T	293 K
Particle Radius	R	0.2 μm (1e-3)

Porfiri.[33] The accumulation of the cations on the cathode and the depletion area at the anode is clearly seen in these results. This occurs as the anions in an IPT are covalently fixed to the polymer matrix. The dielectric constant $\varepsilon\varepsilon_0$ is decreased from 17.7 to 1.77 mF/m for all the remaining numerical simulations. Wallmersperger *et al.*[24] demonstrated that more charges accumulate at the anode for a higher dielectric permittivity. It is noticed from Figs. 3(a) and 3(b) that the accumulation of cations on the cathode is approximately 5% the length of the transducer. The electrode thickness in IPTs is usually 25 μm which consists of 12.5% its total length. If the dielectric constant is kept at 17.7 mF/m the depletion and accumulation regions will cover the electrode area and the effect of adding particles will be diminished. The large dielectric constant value used in Wallmersperger *et al.*[28] is to compensate for absence of particles. Figure 4(a) demonstrates that a total number of 1800 degrees of freedom are needed before a converged steady-state charge is reached.

To capture the effect of the particles in the electrodes, a two-dimensional model is required.

The latter is built and compared against the results of the one-dimensional model. The optimization of mesh parameters for the two-dimensional model is shown in Fig. 4(b). After convergence the steady-state charge for the one- and two-dimensional models are 65.12 and 65.14 C/m^2, respectively. The normalized spatial charge density of the two-dimensional model is perfectly overlapping the calibrated one-dimensional result as shown in Figs. 3(c) and 3(d) for the cathode and anode, respectively.

The final step of the model calibration is to add particles and check for convergence of the steady-state charge density. This step is done with one particle added on each side of the electrode, and the mesh parameters are fine tuned until convergence is reached as shown in Fig. 4(c). Due to computational limitations the size of the particle is set to a circle of radius of 10^{-3} in nondimensional parameters resulting in 0.2 μm if the simulated polymer is 200 μm thick. The particles usually used in IPTs are approximately two orders of magnitude smaller. However, a further decrease in the size of the particles would lead to a drastic increase in the total number of degrees of freedom of the system. In fact, 220 000 degrees of freedom are required for a single particle on each of the electrodes, whereas 2.5×10^6 degrees of freedom are needed for 156 particles. For this work, a workstation with 32 GB of RAM is used and its full memory capacity is reached for the case of 156 particles.

IV. NUMERICAL SIMULATION

In contrast with the literature, where most physics based models simulate the high surface electrodes by prescribing conventional flat electrodes with an increased permittivity ε_r at the polymer boundary, in this paper the high surface electrodes are modeled as porous electrodes. Different small sections in the electrode region are distinguished as: bound charged groups with variable electric potential and regions with prescribed electric potential and no bound charges. Figure 1(a) shows a schematic of an IPT strip revealing the uniformly distributed fixed anions while the mobile cations are aggregating toward the cathode. Figure 1(b) shows a schematic of a typical electrode of an ionic polymer transducer presenting the particles, the flat gold electrode, and the cations accumulating around the particles.

In Fig. 5, the steady-state results at time $t = 10$s of the numerical simulation of the porous electrode with 6 particles is depicted. Figure 5(a) shows the steady charge (ρ/Fc^-) for an applied potential of 50 mV across the electrodes. The steady-state electric potential inside the polymer is shown in Fig. 5(b). It could be seen that the electric voltage on the particles is prescribed to 50 mV and 0mv on the anode and cathode sides, respectively. Figure 5(c) shows the steady-state charge for an applied potential of 500 mV across the electrodes. As compared to Fig. 5(a) the distribution of the charge between the anode and the cathode is highly asymmetric with a large depletion area at the anode. At larger potentials a depletion region is formed at the cathode due to the fact that the anions are fixed to the polymer membrane while the cations are free to move. A similar result has been previously

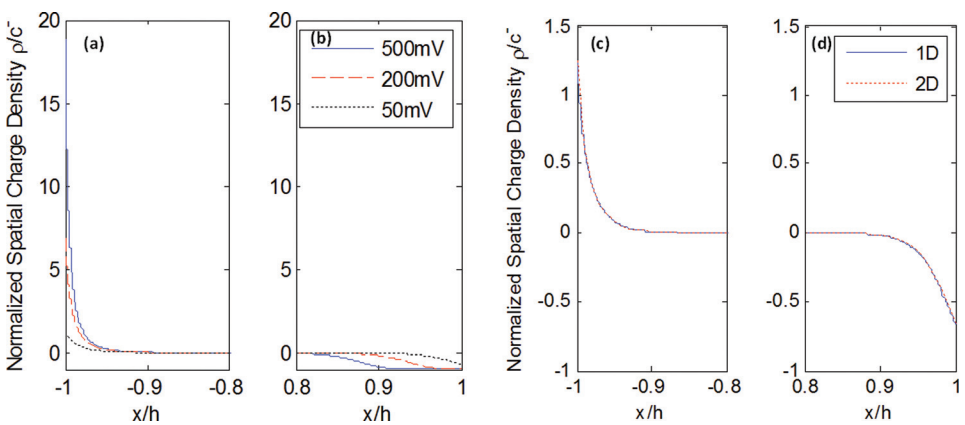

FIG. 3. (Color online) Normalized charge density (a) at the cathode (b) at the anode of a one-dimensional model under the applied potential of 50, 200, and 500 mV, (c) at the cathode and (d) at the anode comparing the one-dimensional model to the two-dimensional model for 50 mV.

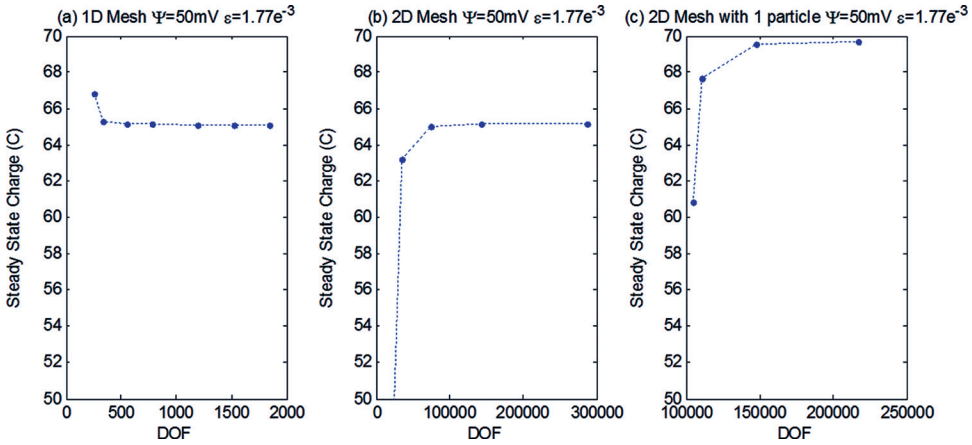

FIG. 4. (Color online) Number of degrees of freedom (DOF) vs the steady-state accumulated charge in Coulombs (a) for the optimization of the 1D mesh parameters for the new case of $\varepsilon = 1.77 \cdot 10^{-3}$, (b) for the 2D mesh parameters, and (c) for the 2D mesh parameters with one particle.

observed in.[15–17] Finally Fig. 5(d) shows the electric field inside the actuator, where it could be observed that the boundary electric potential at the anode is overlapping some of the particles.

In Figs. 6(a) and 6(b) the effect of adding particles on the current passing through the ionic polymer actuator and charge accumulated at the electrodes is studied. Figure 6(a) depicts the current for flat electrodes, 24 particles, and 70 particles. It could be noticed that the peak current is slightly increasing with the addition of particles while the decay time of the curve becomes significantly larger. Figure 6(b) depicts the charge density accumulating at the electrode. It is noticed that adding particles leads to a significant increase in the steady-state charge accumulation.

Next, the effect of increasing the thickness of the electrode T_e while maintaining a constant particle density is studied. For this simulation 25, 50, and 75 particles are uniformly distributed on a larger area with a constant density. For example, the 25 particles are distributed over 5% of the total length (T_e/h) of the polymer while the 50 and the 75 particles covered approximately 10% and 15% of the total length of the actuator, respectively. This resulted in electrodes with constant particle density and a variable thickness. Hence the legend of Fig. 6(c) corresponds to the coverage percentage. The current and charge density are shown in Figs. 6(c) and 6(d) respectively. It is noticed that the thicker the electrode the more charges will accumulate.

To assess the effect of adding particles on the steady-state charge, several numerical simulations with increasing number of particles in the electrode are performed. The result of all these simulations is shown in Fig. 7. It could be

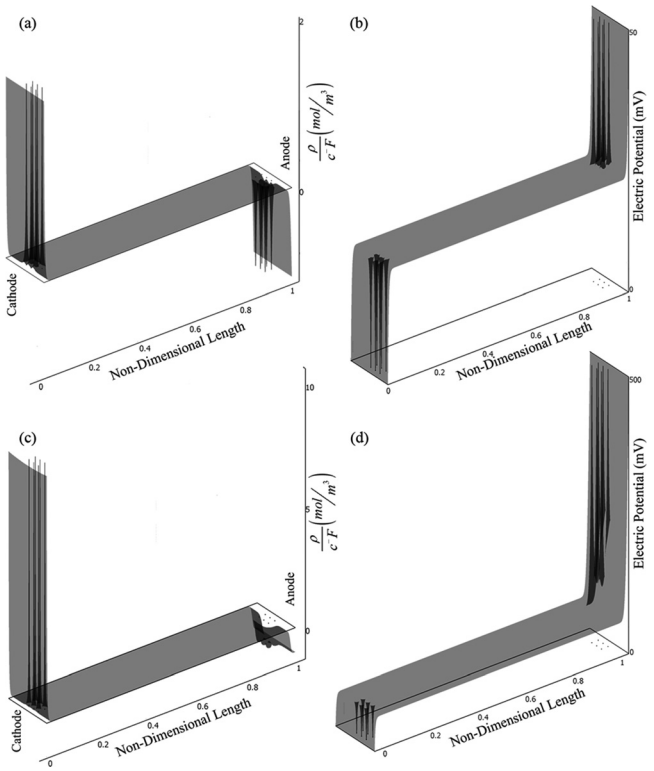

FIG. 5. Three dimensional plot of the (a) steady-state spatial charge distribution; (b) electric potential for an applied voltage of 50 mV; (c) steady-state spatial charge distribution; and (d) electric potential for an applied voltage of 500 mV.

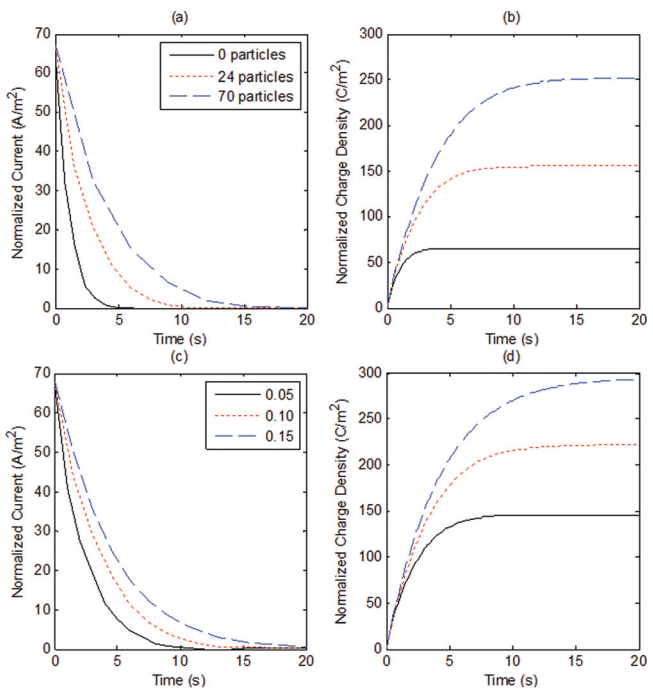

FIG. 6. (Color online) (a) Normalized current depicting the effect of adding particles, (b) the corresponding normalized accumulated charge density, (c) normalized current depicting the effect of thickening the electrode, (d) corresponding charge density.

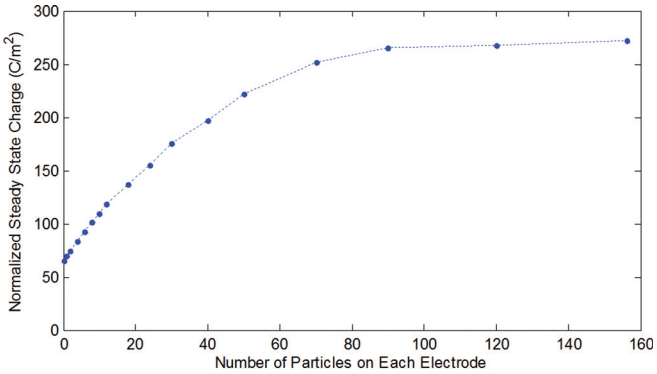

FIG. 7. (Color online) Normalized steady-state charge as a function of the number of particles added at each side of the electrode ($\Psi = 50\text{mV}$).

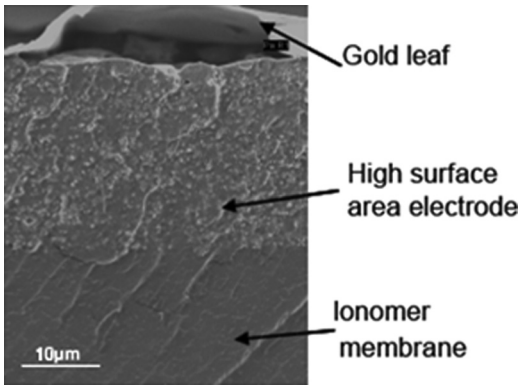

FIG. 8. SEM image of the upper electrode of a typical ionic polymer transducer fabricated using the DAP.

clearly seen that by adding particles, the charge accumulation increases until it reaches an asymptotic value for approximately 100 particles (for the simulation parameters presented in this paper).

V. EXPERIMENTAL METHODS

The numerical model presented earlier is validated using experimental data. For this purpose an experimental setup is built and several ionic polymer actuators were tested. The ionomer chosen in this study is Nafion and the electrode conductor is the high surface area RuO_2 powder particles. It is well documented that the electroding of the IPT actuator is very important to its performance as an actuator.[34,35] The transducers in this study are assembled using the Direct Assembly Process (DAP) since it provides control over the electrode architecture.[36] As mentioned in the introduction an ionic polymer transducer consists of an ionomer membrane sandwiched between two layers of high surface area electrodes. The high surface area electrode is made of a mixture of electrically conductive particles uniformly distributed in an ionomer matrix. In the next section the electrical characterization setup is presented.

A. Direct assembly process

In ionic polymer transducers, high surface area electrodes are required for proper operation. This high surface area electrode is fabricated in this study from a mixture of RuO_2 and Nafion using the novel DAP fabrication method.[36] The DAP consists of imbibing an ionomer membrane in the desired diluent. Bennett and Leo[7] demonstrated that EMI-Tf ionic liquid is an air stable diluent and provides repeatable results, and hence will be used in the experiments of this study. After the ionic liquid is imbibed into the Nafion 117 membrane, the electrodes are applied using a conductive powder painting technique. A polymer/conductor solution is prepared containing a mixture of ionomer solution and the desired conducting powder. This solution is painted directly onto each surface of the solvent containing ionomer membrane. The alcohol solvents and water are removed by heating the membrane under an infra-red lamp during the painting process. The number of layers applied to each side of the membrane control the thickness of the electrode. After the application of the ionomer/conducting powder composite, the sample is sandwiched between two 100 nm thin conductive gold foils and the three layers of the composite are fused together by a hot-pressing process. A SEM image of the cross section of the upper of a typical ionic polymer transducer fabricated using the DAP is shown in Fig. 8.

For this study, six samples are built; four of which had 45 vol% RuO_2 in the electrode, the fifth had 30% RuO_2, and the last 60% RuO_2. The ionic polymer transducers with electrodes composed of 45 vol% RuO_2 had a varied thickness of 10, 25, 30, and 40 μm. The remaining 30 vol% and 60 vol% samples had electrode thickness of 30 μm.

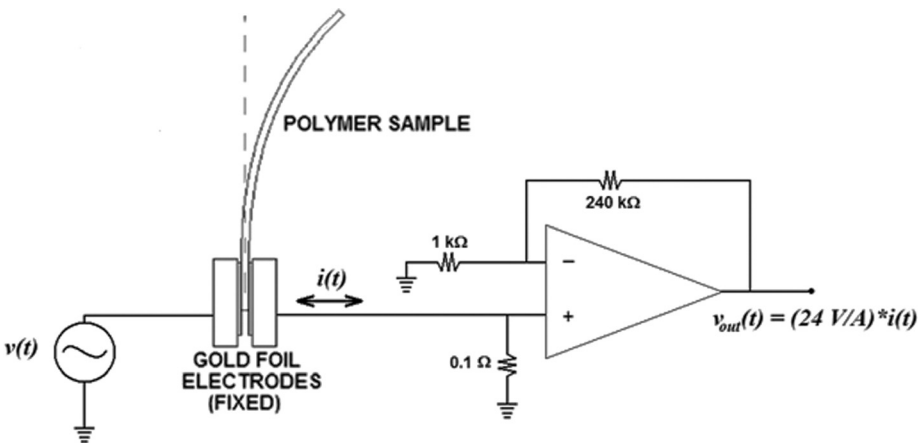

FIG. 9. Current measuring circuit.

B. Impedance characterization

To characterize the current response, a step voltage input was applied to the samples. And the current flowing into the IPT actuator was measured using an in-house made current sensing circuit shown in Fig. 9. The charge is calculated by integrating the current with respect to time.

VI. EXPERIMENTAL RESULTS

In this section, the results of the experimental investigations are presented. A step voltage of magnitude 1 V is applied to the six samples with different electrode architectures and the current is measured using the setup presented in the previous section. In Figs. 10(a) and 10(b), the current and the charge density are respectively shown for the high surface electrodes containing concentrations of particles of 30, 45, and 60 vol% RuO_2. The electrode thickness of these three samples is controlled to be 30 μm. The experimental data demonstrates that the charge density is increased for higher volume percent of particles in the electrode. In Figs. 10(c) and 10(d), the current and the charge density are respectively depicted for high surface electrodes with thicknesses of 10, 25, and 40 μm. The electrode composition is 45% RuO_2 for all these three samples. As shown in the figure, the charge density is increasing with thicknesses.

Comparing the numerical results presented in Sec. IV with experiments one can conclude that the trends are in agreement. The numerical results demonstrate that increasing the particle concentration at constant electrode thickness or increasing the electrode thickness at constant particle density results in more charge accumulation.

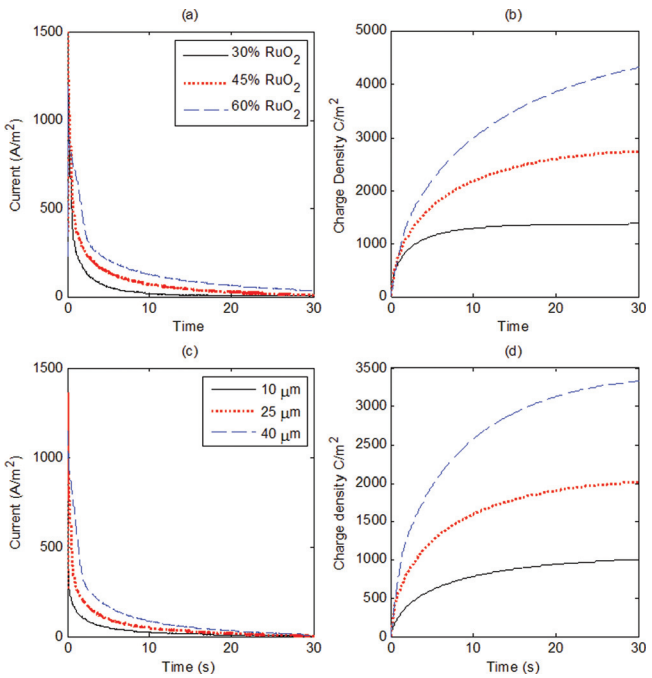

FIG. 10. (Color online) (a) Measured current, (b) charge density for electrodes with thickness of 30 μm containing concentrations of 30%, 45%, and 60% RuO_2, (c) measured current, and (d) charge density for thicknesses of 10, 25, and 40 μm and a concentration of 45% RuO_2.

Memory limitations prohibited matching the magnitudes of the numerical results to the experimental ones. (The machine used in this work has 32 GB of RAM.) In fact, the one order of magnitude discrepancy between the experimentally measured and numerically simulated charge density is mainly due to the lower applied potential. In the experiment, a 1 V step potential is applied which is usually the potential an IPT actuator is characterized and operated at. On the other hand, in the numerical simulation the applied potential is limited to 50 mV in order to avoid sharp gradients in the solutions of the electric potential and ion concentration. The maximum steady state charge density obtained in the numerical simulation is 275 C/m^2 as compared to a maximum of 3300 C/m^2 in the experiment. Previous research indicates that an increase in the applied potential from 0.1 to 1 V results in an increase in peak current from approximately 5 mA/cm^2 to 45 mA/cm^2, and an increase in the charge density from 0.05 C/m^2 to 0.25 C/m^2 (see Fig. 4 in Ref. 24). This also justifies the discrepancy in current density of factor 23 between numerical and experimental results. Furthermore the dielectric constant adopted in this study of 1.77 mF/m is large as compared to that of water; this is limited by the number of particles to be added in the high surface electrode.

Despite the discrepancy in the magnitude of the applied potential, the numerical data follows well the trends of the experimental. At 1 V the dry IPTs characterized in this study does not demonstrate significant nonlinear behavior.[7]

VII. CONCLUSION

The study presented in this paper gives a physics based finite element model that simulates the electro-chemical coupling in ionic polymer transducers. The model consists of a convection-diffusion equation describing the chemical field as well as a Poisson equation describing the electrical field. This numerical model is expanded to two dimensions including the addition of particles. This is the first electro-chemical model accounting for high surface area electrodes in ionic polymer transducers. The model is calibrated against published results. Furthermore, a convergence test is performed for the two-dimensional model with particles, and the appropriate number of mesh elements is selected. The numerical investigations are verified as well by comparison with experimental data. Several transducers are fabricated using the DAP process on Nafion 117 membranes. The architecture of the high surface area electrodes in these samples is varied. The concentration of the high surface area RuO_2 particles is varied from 30 vol% up to 60 vol% at a fixed thickness of 30 μm, while the overall thickness of the electrode is varied from 10 μm up to 40 μm at a fixed concentration of 45%. The flux and charge accumulation in the materials are measured experimentally and compared to the results of the numerical simulations. Computational limitations made it difficult for this model to match the magnitudes of both currents and charge densities. In fact, the memory capacity is limiting the ability to match the applied potential in both numerical and experimental results. On the other hand, trends of the experimental and numerical investigations are in

agreement. These trends demonstrate that by adding more particles to the electrodes, the charge accumulation increases.

[1]K. Oguro, Y. Kawami, and H. Takenaka, J. Micromachine Society Soc. **5**, 27 (1992).
[2]K. Sadeghipour, R. Salomon, and S. Neogi, Smart Mater. Struct. **1**, 3445 (1992).
[3]M. Shahinpoor, Y. Bar-Cohen, J. Simpson, and J. Smith, Smart Mater. Struct. **7**(6), R15 (1998).
[4]*Electroactive Polymer Actuators as Artificial Muscles*, 2nd ed., edited by Y. Bar-Cohen (SPIE Press, Bellingham, 2004).
[5]B. J. Akle and D. J. Leo, Journal of Intelligent Material Systems and Structures **19**(8), 905 (2008).
[6]B. J. Akle, M. D. Bennett, and D. J. Leo, Sensors and Actuators A: Physical **126**(1), 173 (2006).
[7]M. D. Bennett and D. J. Leo, Sensors and Actuators A: Physical **115**, 79 (2004).
[8]B. J. Akle, S. Nawshin, and D. J. Leo, Smart Mater. Struct. **16**, S256 (2007).
[9]B. J. Akle, M. A. Hickner, D. J. Leo, and J. E. McGrath, J. Mat. Sci. **40**(14), 3715 (2005).
[10]R. Kanno, S. Tadokoro, T. Takamori, and M. Hattori, *Linear approximate dynamic model of icpf actuator*, in Proceedings of the IEEE International Conference on Robotics and Automation, pp. 219–225 (1996).
[11]K. M. Newbury and D. J. Leo, Journal of Intelligent Material Systems and Structures **14**(6), 333 (2003).
[12]K. M. Newbury and D. J. Leo, Journal of Intelligent Material Systems and Structures **14**(6), 343 (2003).
[13]S. Nemat-Nasser and Y. Wu, J.Appl. Phys. **93**, 5255 (2003).
[14]S. Nemat-Nasser, S. Zamani, and Y. Tor, J. Appl. Phys. **99**, 104902 (2006).
[15]S. Nemat-Nasser, J. Appl. Phys. **92**(5), 2899 (2002).
[16]T. Wallmersperger, B. Kröplin, and R. W. Gülch, "Modelling and Analysis of Chemistry and Electromechanics," in *Electroactive Polymer (EAP) Actuators as Artificial Muscles - Reality, Potential, and Challenges*, 2nd ed. (SPIE Press, Bellingham, 2004), Vol. PM136, pp. 335–362.
[17]L. M. Weiland and D. J. Leo, J. Appl. Phys. **97**, 013541 (2005); also selected for publication in the Virtual Journal of Nanoscale Science and Technology.
[18]L. M. Weiland and D. J. Leo, J.Appl. Phys. **97**, 123530 (2005).
[19]B. J. Akle and D. J. Leo, Smart Mater Struct. **16**, 1348 (2007).
[20]G. Del Bufalo, L. Placidi, and M. Porfiri, Smart Mater Struct. **17**(4), 0964 (2008).
[21]K. Asaka and K. Oguro, J.Electroanalytical Chem. **480**(1–2), 186 (2000).
[22]Z. Chen, D. R. Hedgepeth, and X. Tan, Smart Mater. Struct. **18**, 055008 (2009).
[23]M. Aureli, W. Lin, and M. Porfiri, J. Appl. Phys. **105**, 104911 (2009).
[24]T. Wallmersperger, B. J. Akle, D. J. Leo, and B. Kröplin, Comp. Sci. Tech. **68**(5), 1173 (2008).
[25]Y. Toi and S. Kang, Comp. Struct. **83**(31–32), 2573 (2005).
[26]M. Porfiri, Phys. Rev. E **79**, 041503 (2009).
[27]T. Wallmersperger, B. Kröplin, and R. W. Gülch, Mech. Mat. **36**(5–6), 411 (2004).
[28]T. Wallmersperger, D. J. Leo, and C. S. Kothera, J. Appl. Phys. **101**(2), 024912 (2007).
[29]T. A. Davis and I. S. Duff, SIAM Journal on Matrix Analysis and Applications **18**(1), 140 (1997).
[30]U. M. Ascher and L. R. Petzold, *Computer Methods for Ordinary Differential Equations and Differential-Algebraic Equations*, 2nd ed. (SIAM, Philadelphia, 1998).
[31]T. J. R. Hughes, *The* Finite Element Method: Linear Static and Dynamic Finite Element Analysis (Dover, New York, 2000).
[32]O. C. Zienkiewicz, R. L. Taylor, and J. Z. Zhu, *The Finite Element Method. Its Basis & Fundamentals*, 6th ed. (Butterworth & Heinemann, England, 2005).
[33]M. Porfiri, J. Appl. Phys. **104**, 104915 (2008).
[34]H. Tamagawa, F. Nogata, T. Watanabe, A. Abe, K. Yagasaki, and J. Y. Jin, J.Mat. Sci. **38**, 1039 (2003).
[35]M. Shahinpoor and K. J. Kim, Sensors and Actuators A **96**, 125 (2002).
[36]B. J. Akle, M. D. Bennett, D. J. Leo, K. B. Wiles, and J. E. McGrath, J.Mat. Sci. **42**(16), 7031 (2007).